UNIVERSITY OF
BATH

Citation for published version:
Edge, KA & Guglielmino, E 2004, 'A controlled friction damper for vehicle applications', Control Engineering Practice, vol. 12, no. 4, pp. 431-443. https://doi.org/10.1016/S0967-0661(03)00119-9

DOI:
10.1016/S0967-0661(03)00119-9

Publication date:
2004

Link to publication

University of Bath

A CONTROLLED FRICTION DAMPER FOR VEHICLE APPLICATIONS

Emanuele Guglielmino†

Centre for Power Transmission & Motion
Control
Department of Mechanical Engineering
University of Bath
Bath BA2 7AY, UK
Email:
emanuele@guglielmino.com

Kevin A. Edge*

Centre for Power Transmission & Motion
Control
Department of Mechanical Engineering
University of Bath
Bath BA2 7AY, UK
Email: K.A.Edge@bath.ac.uk
Fax: +44 1225 386963

ABSTRACT

This paper examines the performance of a servo-driven dry-friction damper in a car suspension application; this device is a potential alternative to a traditional viscous damper. The friction damper is semi-active: damping is controlled without energy introduction into the system and hence the power required is much smaller than fully active systems. Models for the friction damper hydraulic drive and vehicle ride are developed. It is shown through simulation and experimental studies that a VSC-controlled friction damper has potentially superior performance to a conventional damper. Limitations of the current design are identified and suggestions for improvements are outlined.

KEYWORDS: Electro-hydraulic systems; Robust control; Semi-active suspension; Variable-structure control; vehicle suspension

NOMENCLATURE

A_p	Actuator piston area
b	Position feedback coefficient
B	Bulk modulus
$\mathbf{C}$, $\mathbf{C_0}$	Damping matrices
C_q	Valve discharge coefficient

*Corresponding author
† Now at Westinghouse Brakes (UK) Limited, PO Box 74, Foundry Lane, Chippenham SN15 1HY

D	Valve bore diameter
$\mathbf{F_d}$	Frictional force vector
$\mathbf{F_n}$	Normal force vector
i	Valve solenoid current
$\mathbf{K}$, $\mathbf{K_0}$	Stiffness matrices
k_{1s}	Valve leakage coefficient
k_{rv}	Relief valve override coefficient
k_s	Suspension stiffness
k_t	Tyre stiffness
k_z	Spool displacement-current gain
M_1	Sprung mass
M_2	Unsprung mass
$\mathbf{M}$	Mass matrix
$\mathbf{P}$	Car geometry matrix
P_t	Return line pressure
P_A	Actuator pressure
P_c	Relief valve cracking pressure
P_s	Supply pressure
$\mathbf{q}$	Lagrangian co-ordinate vector
Q_1, Q_3	Flow through the valve
Q_2	Compressibility flow in the actuator
Q_c	Compressibility flow in the supply line
Q_p	Pump flow
Q_{rv}	Flow through the relief valve
s	Laplace operator
T	Frictional memory lag
u	Valve lap
V_{hose}	Supply line volume
V_t	Actuator volume
x	Relative displacement between sprung and unsprung masses

x_1	Absolute sprung mass displacement
x_2	Absolute unsprung mass displacement
y	Valve spool displacement
z	Valve spool displacement
$\mathbf{z}$	Vertical displacement vector
$\mathbf{z_0}$	Road input vector
z_0	Road input
μ	Friction coefficient
ρ	Hydraulic oil density
ξ	Quarter car damping ratio
ξ_v	Valve damping ratio
ω_n	Valve natural angular frequency
ω_1	Sprung mass natural angular frequency

1. INTRODUCTION

The fundamental goal of any suspension system is the isolation of a structure from external excitation. In the case of a vehicle, a classical car suspension aims to achieve isolation from the road by means of a spring type element and a viscous damper. The characteristics of the elements of the suspension are chosen according to comfort, road holding and handling specifications. A suspension unit should to be able to reduce chassis acceleration as well as dynamic tyre force within the constraints of a set working space and with minimal energy consumption.

Passive suspensions have inherent limitations as a consequence of the trade-off in the choice of the spring rate and damping characteristics, in order to achieve acceptable behaviour over the whole range of working frequencies. This has motivated the investigation of controlled suspension systems, where spring-like and the damper-like characteristics are obtained through the adoption of either semi-active or active suspensions. In a semi-active suspension the damper is replaced by a controlled dissipative element and no energy is introduced into the system. In contrast, an active suspension involves the use of a fully active actuator, and a significant energy input is generally required.

Controlled suspensions (both active and semi-active) have considerable appeal to automotive engineers. A variety of designs and related control schemes have been proposed over the years. The first paper on the topic dates back to 1954 (Federspiel-

Labrosse). A review of the state-of-the-art of controlled suspensions has been carried out by Hedrick and Wormely (1975) and by Goodall and Kortüm (1983). Sharp and Crolla (1987) and Crolla and Aboul Nour (1988) produced comparative reviews of the advantages and drawbacks of various types of suspensions. Another historical review and also an attempt to present some design criteria was given by Crolla (1995). Hillebrecht et al (1992) from BMW have discussed the trade-off between customer benefit and technological challenge from the angle of a car manufacturer. Semi-active suspensions were first introduced in the 1970s, (Crosby and Karnopp, 1973) as an alternative to the costly, complicated and power demanding active systems. A comparative study with passive systems was carried out by Margolis (1982) and by Ahmadian and Marjoram (1989). As with active systems, a variety of control schemes have been proposed for semi-active suspensions: adaptive schemes (Bellizzi and Bouce, 1989); optimal control (Tseng and Hedrick, 1994); LQG schemes (Barak and Hrovat, 1988) as well as robust algorithms (Choi et al, 2000). Many schemes are based on studies using car models of various degrees of sophistication, but the actuator dynamics have not always been modelled adequately. This weakness has been addressed by several authors, including Miller (1988) who analysed the effects of hardware limitations.

In this work the controlled damping element is a frictional damper. This is a device which conceptually is composed of a plate fixed to a moving mass and a pad pressing against it. A schematic of its physical principle is depicted in figure 1. An external normal force F_n is applied to a mass by the pad and consequently, in the presence of a relative motion between the pad and the plate, a frictional damping force F_d is produced. The choice of using dry friction as a mean of achieving a damping effect is non-conventional, particularly in an automotive application. Pure dry (or lubricated) friction characteristics are of no practical use because of their harshness, but a controlled friction damper can be made to behave in a variety of ways emulating spring-like and pseudo-viscous characteristics.

2. MODEL OF THE SYSTEM

The system studied is depicted in figure 2. It is composed of two main functional blocks: the car and the controlled friction damper. The friction damper is force controlled. This is achieved by means of an electrohydraulic servo-actuator system. An electrohydraulic proportional underlapped valve is supplied by a pump in parallel with a relief valve and drives a single-chamber actuator under pressure control. The hydraulic valve essentially behaves in a manner analogous to a potential divider in an electrical circuit. The car is modelled initially via a 2 DOF quarter car model for the purpose of preliminary controller design.

The quarter car equipped with the friction damper is described by the following expressions:

$$M_1 \ddot{x}_1 = -F_d - 2\xi\omega_1 M_1(\dot{x}_1 - \dot{x}_2) - k_s(x_1 - x_2) \tag{1a}$$

4

$$M_2 \ddot{x}_2 = F_d + 2\xi\omega_l M_l(\dot{x}_l - \dot{x}_2) + k_s(x_l - x_2) - k_t(x_2 - z_0) \qquad (1b)$$

In general, the relationship between F_d and F_n is:
$$F_n = F_n(x, \dot{x}, \ddot{x}_l, P_A)H(P_A) \qquad (2)$$

where $x = x_l - x_2$ and $H(\cdot)$ is the Heavyside step function. The friction model employed was identified by measuring the actual friction force produced on the friction damper designed. Measurements (Guglielmino, 2001) showed that the friction force can be modelled statically with Coulomb friction, and dynamically, in response to changes in the sign of velocity, with a pure frequency-independent delay (known as "frictional memory", Armstrong-Helouvry et al, 1994). Stiction was found to be negligible, and therefore the friction model employed is:

$$F_d(t) = -\mu F_n(t-T)sgn(\dot{x}_l - \dot{x}_2) \qquad (3)$$

For validation purposes a 7 DOF vehicle ride model (Wong, 1993) has been developed; it allows 3 DOF (bounce, roll and pitch) for the sprung mass and 4 DOF for the unsprung mass (figure 3). Front suspensions are taken to be independent and rear suspensions are dependent (connected via a rigid axle). This model is consistent with the experimental investigations undertaken on a car. The model is described by the following equation (bold letters denote matrices and vectors):

$$\boldsymbol{M\ddot{q}} + \boldsymbol{P^T CP\dot{q}} + \boldsymbol{P^T KPq} + \boldsymbol{F_d} = -\boldsymbol{P^T K_0 z_0} - \boldsymbol{P^T C_0 \dot{z}_0} \qquad (4)$$

with $\boldsymbol{q} \in \Re^7$, $\boldsymbol{z_0} \in \Re^4$, $\boldsymbol{F_d} \in \Re^7$, $\boldsymbol{M} \in \Re^{7 \times 7}$, $\boldsymbol{K} \in \Re^{8 \times 8}$ and $\boldsymbol{C} \in \Re^{8 \times 8}$ $\boldsymbol{K_0} \in \Re^{8 \times 4}$, $\boldsymbol{C_0} \in \Re^{8 \times 4}$ and $\boldsymbol{P} \in \Re^{8 \times 7}$. The vertical displacement vector $\boldsymbol{z} \in \Re^8$ is defined as:

$$\boldsymbol{z} = [z_l, z_2, z_3, z_4, z_5, z_6, z_7, z_8]^T \qquad (5)$$

$\boldsymbol{z}$ and $\boldsymbol{q}$ being related by the matrix $\boldsymbol{P}$:

$$\boldsymbol{z} = \boldsymbol{Pq} \qquad (6)$$

The electrohydraulic servo-system is modelled by consideration of flow continuity and actuator force balance. An equivalent hydraulic circuit for flow continuity assessment is shown in figure 4. The pump flow continuity equation is:

$$Q_p = Q_l + Q_{rv} + Q_c \quad \text{for} \quad P > P_c \qquad (7)$$

(and $Q_p = Q_l + Q_c$ for $P < P_c$. However in the model the pump is taken to supply enough flow so as to keep the relief valve always open).
The governing equation of the relief valve is:

$$P_s = P_c + k_{rv}(Q_p - Q_l - Q_c) \qquad (8)$$

The compressibility flow in the connecting hose is:

$$Q_c = \frac{V_{hose}}{B} s P_s \qquad (9)$$

Applying the continuity equation at the second node of the circuit of figure 4, yields:

$$Q_1 = Q_2 + Q_3 \qquad (10)$$

An appropriate model of the valve is necessary. Because the valve works in pressure control mode and therefore around the spool central position, the leakage flows play a major role in defining the slope of the pressure gain characteristic (i.e. the relationship between pressure and valve-opening when the outlet port is blocked). This characteristic has a significant impact on the overall performance of the controller. Depending upon the length of the leakage flow path, the flow regime can be either laminar, turbulent or transitional. The model proposed by Eryilmaz and Wilson (2000) which assumes turbulent flow and an empirical correlation to model the effects of valve opening has been adopted here. Using the notation shown in figure 5, the flow Q_1 is given by:

$$Q_1 = C_q \pi D (u+z) \sqrt{\frac{2(P_s - P_A)}{\rho}} \qquad \text{if } z \geq 0 \qquad (11a)$$

$$Q_1 = C_q \pi D \sqrt{\frac{2(P_s - P_A)}{\rho}} \frac{u^2}{(u - k_{1s}z)} \qquad \text{if } z < 0 \qquad (11b)$$

Because the motion of the friction pad is very small the actuator can be modelled as a chamber of fixed volume (V_t) containing a compressible liquid with a bulk modulus of elasticity, B. Hence,

$$Q_2 = \frac{V_t}{B} s P_A \qquad (12)$$

The flow Q_3 is modelled in an identical manner to the flow Q_1:

$$Q_3 = C_q \pi D \sqrt{\frac{2(P_A - P_t)}{\rho}} \frac{u^2}{(u + k_{1s}z)} \qquad \text{if } z \geq 0 \qquad (13a)$$

$$Q_3 = C_q \pi D (u-z) \sqrt{\frac{2(P_A - P_t)}{\rho}} \qquad \text{if } z < 0 \qquad (13b)$$

with $-u \leq z \leq u$

where $k_{1s} = \frac{1}{2} \sqrt{\frac{P_s + P_A(u) - P_t}{P_s - P_A(u) - P_t}} - 1 \qquad (14)$

Spool-solenoid electromechanical dynamics are closely approximated by a second-order linear model described by:

$$\frac{z}{i}(s) = \frac{k_z}{\dfrac{s^2}{\omega_n{}^2} + 2\dfrac{\xi_v}{\omega_n}s + 1} \qquad (15)$$

The valve amplifier voltage-current dynamics are fast enough to be neglected.
Finally, the force balance (taking actuator piston acceleration as negligibly small) is:
$F_n = P_A A_P$ (16)

3. CONTROLLER DESIGN

Although various standards exist, ride comfort is not easy to quantify because it is inherently a subjective matter. Several criteria have been proposed based on minimising different combinations of position, velocity, acceleration and jerk; a useful review of the literature is provided by Guglielmino (2001). For this work it was decided to reduce chassis acceleration as this is generally accepted as a key attribute in achieving comfort. To achieve this goal the controller was designed with the aim of tracking spring force and is meant to work most effectively in the neighbourhood of the chassis resonance (typically around 1.5 Hz).

Initially sliding mode control of cylinder *pressure* was investigated by the authors (Guglielmino and Edge, 2000) (the valve pressure gain characteristic inherently constitutes a sliding mode controller with boundary layer). However in this scheme chattering was too large and in a car suspension application this could not be tolerated. Consequently a proportional-type VSC rather than a switching-type VSC was considered. However, the semi-active friction device has an inherent physical limitation: it can only oppose to the motion and not assist it and therefore it is not possible to apply the control force continuously, but only when the following condition is met [obtained from Lyapounov stability theory (Guglielmino and Edge, 2000 and Guglielmino and Edge, 2001)]:

$x\dot{x} \leq 0$ (17)

(otherwise the control force would have the same direction of the spring force).

In order to achieve spring force tracking, the control action must be proportional to the elastic force, hence:

$F_n = b\,k_s\,|x|$ if $x\dot{x} \leq 0$ (18a)
$F_n = 0$ if $x\dot{x} > 0$ (18b)

This is also known as "balance" logic (Stammers and Sireteanu, 1997; Guglielmino, Stammers and Edge, 2000) since it actually balances the spring force by trying to produce an opposite control force which cancels it. The coefficient *b* is a gain defining the level of cancellation of the spring force, inversely proportional to the friction coefficient. Assuming that the friction coefficient is perfectly known (and

working on the assumption of pure Coulomb friction), then in order to obtain perfect spring force cancellation, $b = \mu^{-1}$. However there will be always a mismatch between the assumed and actual friction coefficients. Hence, in practice, the coefficient b $= \mu_{assumed}^{-1}$ and the actual degree of spring cancellation will be dictated by the ratio $\mu / \mu_{assumed}$. Strictly, the tracking law ought to take into account the hydraulic system dynamic behaviour. However this would result in a very complicated control law with questionable benefit. Provided that hydraulic dynamics are fast enough, it should be possible to reduce RMS values of the overall response, rather than perform perfect instantaneous tracking.

Equation (18) can be written as:

$$F_n = \frac{bk_s}{2} \left| x \right| - \frac{bk_s}{2} \left| x \right| sgn(x\dot{x}) \tag{19}$$

By substituting for F_n in equation (3) and noting that $\left| x \right| sgn(x\dot{x}).sgn(\dot{x}) = x$, the friction force can be expressed by equation 20 (to simplify the notation the time delay T is omitted in the subsequent equations):

$$F_d = -\frac{\mu bk_s}{2} xsgn(x\dot{x}) + \mu \frac{bk_s}{2} x \tag{20}$$

Therefore controller (20) is composed of a switching term and a state feedback term. The product $(x\dot{x})$ can be interpreted as a particular nonlinear sliding surface. With this strategy the valve mainly works in the (near) linear zone of its pressure gain characteristic, as opposed to sliding mode control where saturation limits would be exploited. Additional viscous damping may be added either in first and third quadrants of the phase plane diagram or in second and fourth quadrants (Guglielmino and Edge, 2001).

Because the system inherently dissipative, it is expected to be stable. Closed-loop asymptotic stability can be formally demonstrated by using Lyapounov's direct method, as described by Guglielmino (2001) .

4. EXPERIMENTAL WORK AND MODEL VALIDATION
4.1 The hydraulic drive

For experimental studies a single friction damper was constructed in such a manner as to be able to replace a conventional viscous damper in a vehicle (figure 6). The embodiment of the concept was a piston in a cylindrical housing which contains two diametrically-opposed pistons upon which are bonded the friction pads. The pistons are supplied with hydraulic oil through the centre of the piston rod, with the control valve mounted remotely.

A potentially major limiting factor in the system is the pressure dynamic response of the valve. In order to establish its bandwidth as well as its pressure gain, a bench test

assessment was undertaken. The experimentation on the valve-actuator system showed an unexpected behaviour at low supply pressure: dynamic performance was extremely poor. Bandwidth was severely limited (around 4 Hz) despite the valve being of a relatively sophisticated design. Figure 7 depicts the frequency response for three different input voltages and with the relief valve cracking pressure set at 10 bar (which was initially chosen as the supply pressure for this application in order to minimise the energy input). The reasons of such a slow response were investigated thoroughly. Investigation of the valve spool dynamics revealed that the valve itself was quite fast (around 100 Hz bandwidth) and was virtually independent of supply pressure. Figure 8 shows the valve spool frequency response for a voltage input (the figure presents the signal from the valve spool displacement transducer). The simulation of a second order linear model with a natural frequency of 105 Hz and a damping ratio of 0.60 matches the results well. Thus the problem of the limited pressure bandwidth was not caused by the valve itself and hence could only be attributed to a fluid mechanics problem. A set of tests was designed to identify the possible cause.

The first hypothesis made was that at low pressure an air pocket could have been trapped inside the valve: at low pressures a small quantity of air enormously reduces bulk modulus which adversely affects the dynamical response of the system. In order to assess this hypothesis, the valve was mounted upright, hence preventing air stagnating close to the load port; the valve was flushed through with oil and immediately afterwards the frequency response was measured. No appreciable change occurred. A second hypothesis was that at low pressure the small pressure drop past the orifice was not sufficient to fully develop the turbulent flow regime. To examine this the valve was driven with a biased signal to create a narrower flow path and hence a larger pressure drop, helping to promote turbulent flow. However there was no improvement in performance. The ripple in the supply pressure was also considered as a possible cause, but it was found to be negligible. It was eventually decided to carry out tests with an increased supply pressure. The bandwidth improved with increasing supply pressure rising to around 20 Hz. With an increase in pressure any free air present is more likely to dissolve into the liquid. Hence the reason of the slow dynamic response is postulated to be due to the presence of air bubbles probably arising from air release occurring within the valve. This would account for flushing of the system with oil being ineffective. Therefore although the system pressure for the application was initially selected to be 10 bar, it was necessary to trade-off between the higher power consumption (associated with the higher pressure) and the valve system bandwidth: as a consequence all subsequent tests on the car were carried out with a supply pressure of 64 bar.

In order to match the simulation to the experimental results, the presence of air in the oil had to be included in the dynamic model. Its effect was accounted for by a dramatic reduction in the effective bulk modulus of the fluid. An exceptionally low bulk modulus of around 5×10^7 N/m^2 (compared to 1.6×10^9 N/m^2 for the oil alone) led to a reasonable agreement between the simulated and experimental responses.

Such a low value is physically possible when air is present (McCloy and Martin, 1980). The pressure vs. valve demand frequency response presented in figure 9 shows close correspondence to a first order system with a dominant pole at around 20 Hz in cascade with the two complex conjugated poles corresponding to the spool dynamics. The volume of oil downstream of the valve has a significant effect on performance. Therefore in a final design the volume should be minimised, with the valve integrated into the assembly such that it is as close as possible to the friction pad piston(s). The impact of additional volume is presented in figure 10. An increase of the volume by an order of magnitude in the simulation model reduces the bandwidth by about a decade. This is consistent with a linearized analysis of the system which shows that the hydraulic time constant is directly proportional to the volume (Guglielmino, 2001).

The other key characteristic to be established is the pressure gain which sets the closed-loop incremental gain and therefore the tracking ability of the controller. The local slope of the pressure gain around the valve null position depends upon the valve underlap u and the leakage coefficient k_{ls}. These two parameters were estimated via a trial and error procedure. Relief valve cracking pressure was taken as 64 bar. The dependence of the pressure gain upon valve lap is shown in figure 11 and compared with that experimentally measured. The upper bound region of the characteristics is affected more by a change in the underlap width than the lower bound region. The asymmetry in the behaviour either side of the null (0 volt) is caused by, inter alia, the leakage term and the relief valve pressure override. Figure 12 depicts the dependence upon the leakage coefficient, which is varied between 0.5 and 2.5 (taking an underlap of 0.1 mm). From consideration of the figure, the best fit is obtained when $k_{ls} = 1.5$.

4.2 Vehicle investigations
For the vehicle studies experiments were conducted on a small family saloon car, firstly in its original state and then with a single friction damper installed in the rear offside suspension replacing the original viscous damper. Simulation studies were also undertaken using the parameters listed in Table 1.

The control valve was located in the boot of the car and was connected as close as possible to the friction damper using a short length of hose to minimise the oil volume. Performance was assessed experimentally by means of a four-axis vertical road simulator. Firstly response of the original car is presented as a benchmark test. The 7 DOF model aims to only represent the vertical dynamics of the car (i.e. ride). Lateral dynamics (i.e. handling) are not considered here. The measured RMS acceleration of the right rear body acceleration for an input excitation of 7 mm is shown in figure 13 (represented by the stars). Predicted behaviour, for four different levels of viscous damping, is also shown. Up to 4 Hz the match is fairly good. At the higher frequencies, simulation overestimates the acceleration. This is principally due to some unmodelled nonlinearities (rather than to neglected dynamics), principally associated with the viscous damper characteristics (the viscous damper characteristics employed in the model were obtained by linearising their actual characteristic around

the origin; the real characteristics are nonlinear with different trends for bound and rebound strokes). Best agreement between predicted and measured behaviour was obtained with a viscous damping coefficient of 400 N/(m/s).

Figure 14 shows the original vehicle rear right body acceleration time history at a frequency of 2.5 Hz (the phase shift is only for graphical clarity). The experimental trend is almost sinusoidal; this confirms the hypothesis that the behaviour of the car is reasonably linear for sufficiently large amplitudes. Under such conditions the simulated behaviour is quite close to the experimental response. The model generally works well for input amplitudes of the order of a centimeter; however, if the inputs are too large or too small they can excite unmodelled dynamics. Therefore, the car model, despite being linear and relatively unsophisticated, captures the main features of the response both in the time domain and in the frequency domain, up to the chassis resonance frequency. For more accurate modelling of the higher frequency range a more complicated model would be required.

For the case of the controlled suspension, figure 15 shows the experimentally determined acceleration transmissibility ratio for an input of 7 mm in the range 1 to 5 Hz compared with the original system. The controlled system outperforms the passive system over most of frequency range considered although the passive system response is marginally better up to 1.8 Hz. The controlled response presents three peaks: the first is the semi-active system chassis resonance, at 1.7 Hz; this frequency is lower than the corresponding passive resonance and its amplitude is smaller. The inferior behaviour of the semi-active system at low frequency is due to the hydraulic circuit back-pressure, which causes a residual constant-amplitude friction force. The small amplitude of the disturbance at the lowest frequencies does not produce very significant pressure variations: in that range the residual friction force is not negligible. As the frequency increases, the friction damper works properly. Hence, the residual friction force leads to a deterioration of the performance of the damper if the disturbance is not large, i.e. on smooth roads and at low speed. A possible remedy would be the compensation of the residual friction force via a pre-loaded spring inside the damper. Two more peaks are evident in the semi-active curve. This is a nonlinear effect of the semi-active system, but in fact the resonances do not create any problem, because they are far lower than the corresponding passive values. In summary, this initial result proves that the controlled semi-active device is effective. Figure 16 portrays the rear-right suspension working space (z_4-z_8) for both cases. Over the frequency range considered the wheel motion can be assumed to be almost steady, hence working space is a good approximation to absolute chassis displacement. The results presented show that the passive response is better. This is because of the force tracking performed by the controller which inherently promotes higher displacements.

Figures 17 and 18 show the effect of a change in the control law and in the friction properties. Figure 17 examines the effect of changing the closed loop coefficient b from 2 to 3.33; because b is the reciprocal of the friction coefficient μ, its increase can be considered as equivalent to a decrease of the friction coefficient from 0.5 to 0.3. The performance with the "reduced" friction shows some deterioration over part of

the frequency range: this is to be expected since with a lower assumed friction coefficient, the force cancellation is smaller, resulting in higher accelerations.

It is worthwhile evaluating how a change in the frictional characteristic would affect the performance of the control scheme. The test results shown in figure 18 were obtained for the case of lubricated friction and are compared to dry friction (the control algorithm for this test also included also a velocity-feedback term and hence the performance is different to that shown in figure 17). This test is important, because lubricated friction is a possible and realistic alternative to pure dry friction: it helps reduce stiction and is potentially advantageous in terms of heat dissipation. At low frequencies dry friction system response is better than the lubricated friction system response although both are worse than the passive response. In the central frequency band lubricated friction response is better, but at highest frequency the dry friction response is superior. In both cases the performance of the controlled suspension is generally better than the passive system.

From the foregoing investigations involving changes in the feedback coefficient b (equivalent to a change in dry friction coefficient), and the nature of the lubrication regime, the insensitivity of the system to these key elements has been clearly demonstrated. Moreover, the semi-active system remains generally superior to the passive system, even in the presence of these changes. A simulation sensitivity analysis was carried out to identify the most suitable values for the critical parameters.

Figure 19 represents the frequency response for different friction coefficients μ between 0.1 and 0.2. At low frequency the trend is virtually independent of the friction coefficient but after the resonance the dependency gets stronger. A smaller friction coefficient produces a large resonance peak but it tracks the experimental response at higher frequency better; and vice-versa for a larger coefficient. Therefore, a trade-off value of 0.15 has been chosen. The mismatch occurring for frequencies higher than 3.8 Hz is due to the limitations in the car model, and the over-simplified model for the other three (passive) dampers, rather than to the hydraulic model of the friction damper. Figure 20 portrays the frequency response for different levels of delay between velocity and friction force created by the frictional memory effect. A change of ±50% does not produce any significant change except at the lowest frequencies.

In figure 21 the effect of a change in the actuator and connecting pipe volume is considered. An increase of an order of magnitude in the volume produces a noticeable effect for frequencies above 2.5 Hz. The impact of the corresponding reduction of the valve-actuator bandwidth, following an increase in volume, is a higher acceleration. Physically this is because the valve-actuator system cannot catch up with the higher frequency disturbance; therefore the effect of the residual constant friction force plays the dominant role.

Figure 22 shows the predicted and measured sinusoidal time response after the start-up transient has decayed. The simulation follows the overall trend of the measured acceleration well. The spikes in the experimental results are not captured by the model, but most of them arise from noise present in the measurements. The overall agreement is considered acceptable.

Figure 23 shows the semi-active experimental system response to a pseudo-random input. The RMS of the acceleration is 0.58 m/s^2, which is smaller than the passive case (0.75 m/s^2). Figure 24 shows the semi-active system response to a sinusoidal bump. The acceleration overshoot and undershoot for the semi-active system are 1.1 m/s^2 and -0.9 m/s^2 whereas for the passive system are ±0.85 m/s^2. The number of oscillations is the same for both cases. Thus the semi-active system is slightly worse in response to a bump. This is because of the relatively slow response of the pressure control circuit. A bump can be thought has a high frequency half-wave input (the higher the velocity, the higher the frequency) and above a certain frequency the servo system response is not fast enough.

5. CONCLUSIONS AND PROPOSALS FOR FURTHER WORK

The objective of this work was to prove the effectiveness of a controlled friction damper as an alternative to a viscous damper in a vehicle suspension application. A variable structure controller has been designed to meet the performance requirements, taking into account the intrinsic physical limitations of the controller.

Models of the hydraulically actuated friction damper and of the vehicle have been developed and system performance predicted using simulation. An experimental validation of the simulation study has been undertaken on the various subsystems and on the whole system. The model of the hydraulic drive describes the measured behaviour very well. The leakage model employed for the valve is effective in predicting the actual pressure gain. The critical phenomenon of the air in the oil, which limits the bandwidth of the system, was taken into account by reducing the effective bulk modulus of the fluid.

It has been shown that a reduction in chassis acceleration can be obtained at the cost of an increase in working space. The control algorithm has been shown to have good robustness properties. The semi-active system model works reasonably well in terms of predicting time domain response. Its frequency response matches the experimental data well up to the chassis resonance; at higher frequencies the results are overestimated because of the limitations of the car model and the use of a linear model for the remaining (conventional) dampers. The acceleration time responses are also accurately predicted.

The major problem that arose in the course of the experimental work was the limited pressure control system bandwidth at low hydraulic supply pressure. This was

unexpected from the initial simulation studies and to achieve a (barely satisfactory) bandwidth necessitated an increase of the supply pressure with a subsequent increase of the power dissipated. The trade-off between power consumption and bandwidth is a serious problem and will be addressed in further studies by consideration of alternative pressure modulation schemes.

The natural extension of what has been done so far is to extend the control to the whole suspension system of the car. This will require the extension of the algorithm to the control of four independent friction dampers, constituting a complete semi-active car suspension. Handling dynamics also need to be explored.

6. REFERENCES

Ahmadian, M. and Marjoram, R.H. (1989). Effects of passive and semi-active suspension on body and wheel-hop control, *SAE Paper N. 892487*.

Armstrong-Hélouvry, B., Dupont, P., and Canudas de Wit, C. (1994). A survey of models, analysis tools and compensation methods for the control of machines with friction, *Automatica,* Vol. 30, No. 7, July 1994, pp. 1083-1138.

Barak, P. and Hrovat, H. (1988). Application of the LQG approach to the design of an automotive suspension for three-dimensional vehicle model, *Proc. IMechE Advanced Suspensions Conference*, London, UK, pp. 11-26.

Bellizzi, S. and Bouce, R. (1989). Adaptive control for semi-active isolators, *ASME-DED-DE,* Vol. 18 (2), pp. 317-323.

Choi, S.B., Choi, Y.T. and Park, D.W. (2000). A sliding mode control of a full-car electrorheological suspension via hardware-in-the-loop simulation, *Journal of Dynamic Systems, Measurement and Control*, Vol. 122, pp. 114-121.

Crolla, D.A. (1995). Vehicle dynamics-theory into practice, *Proc. IMechE*, Part D: Journal of Automobile Engineering, Vol. 210, No.2, pp. 83-94.

Crolla, D.A. and Aboul Nour, A.M.A. (1988). Theoretical comparisons of various active suspension systems in terms of performance and power requirements, *Proc. IMechE, Advanced Suspensions Conference*, London, pp. 1-9.

Crosby, M.J. and Karnopp, D.C. (1973). The active damper-a new concept for shock and vibration control, *The Shock and Vibration Bulletin*, N. 43, part 4, pp. 119-133.

Eryilmaz, B. and Wilson, B.H. (2000). Modeling the internal leakage of hydraulic servovalves, *ASME IMECE 2000*, Orlando 2000, USA.

Federspiel-Labrosse, G.M. (1954). Contribution a l'etude et au perfectionement de la suspension des vehicules, *J. de la SIA, FISITA*, pp. 427-436.

Goodall, R.M., and Kortüm, W. (1983). Active control in ground transportation-a review of the state-of-art and future potential, *Vehicle System Dynamics*, Vol. 12, pp. 225-257.

Guglielmino, E. (2001). Robust control of a hydraulically actuated friction damper for vehicle applications. PhD Thesis, University of Bath, UK.

Guglielmino, E., Stammers, C.W. and Edge K.A. (2000). Robust force control in electrohydraulic friction damper systems using a variable structure scheme with non linear state feedback, *2nd IFK*, Dresden, Germany.

Guglielmino, E. and Edge, K.A. (2000). Robust control of electrohydraulically actuated friction damper, *ASME IMECE 2000*, Orlando, USA.

Guglielmino, E. and Edge, K.A. (2001). Modelling of an electrohydraulically-activated friction damper in a vehicle application, *ASME IMECE 2001*, 11-16 November 2001, New York, USA.

Hedrick, J.K. and Wormely, D.N. (1975). Active suspension for ground support vehicles - a state-of-the-art review, *ASME-AMD*, Vol. 15, pp. 21-40.

Hillebrecht, P., Konik, D., Pfeil, D, Wallentowitz, H., & Zieglmeier, F. (1992). The active suspension between customer benefit and technological competition. *Proc. IMechE - XXIV FISITA Congress*, London (UK), pp. 221-230.

McCloy, D. and Martin, H.R. (1980). *Control of Fluid Power - Analysis and Design*, 2nd Ed., Ellis Horwood.

Margolis, D.L. (1982). The response of active and semi-active suspensions to realistic feedback signals, *Vehicle System Dynamics*, Vol. 11, No.3. pp. 267-282.

Miller, L.R. (1988). The effects of hardware limitations on an "On/Off" semi-active suspension, *Proc. IMechE Advanced Suspensions Conference*, London, UK, pp. 199-206.

Sharp, R.S. and Crolla, D.A. (1987). Road vehicle suspension system design-a review, *Vehicle System Dynamics*, Vol. 16, pp. 167-192.

Stammers, C.W. and Sireteanu, T. (1997). Vibration control of machines by using semi-active dry friction damping, *Journal of Sounds and Vibrations*, 209(4), pp. 671-684.

Tseng, H.E. and Hedrick, J.K. (1994). Semi-active control laws - optimal and sub-optimal*, Vehicle System Dynamics*, Vol. 23, pp. 545-569.

Wong, J.Y. (1993). Theory of ground vehicles, Wiley.

Table 1: Key parameters used in simulation

Friction damper and hydraulic drive parameters

PARAMETER	VALUE
Underlap (u)	0.1 [m]
Actuator area (A)	6.28×10^{-4} [m^2]
Pump flow (Q$_p$)	9×10^{-5} [m^3/s]
Cracking pressure (P$_c$)	64 [bar]
Relief valve override (k$_{rv}$)	10^4 [bar.s/m^3]
Chamber volume (V$_t$)	10^{-4} [m^3]
Connecting hose volume (V$_{hose}$)	10^{-3} [m^3]
Bulk modulus (B)	1.6×10^9 [N/m^2](supply) 5×10^7[N/m^2] (actuator)
Discharge coefficient (C$_q$)	0.62 [-]
Leakage coefficient (k$_{1s}$)	1.5 [-]
Valve spool damping ratio	0.6 [-]
Valve spool resonance frequency	105 [Hz]
Hydraulic oil density	870 [kg/m^3]
Friction coefficient	0.4 [-]
Frictional memory	10^{-2} [s]

Quarter car model parameters

PARAMETER	VALUE
Sprung Mass (M$_1$)	165 [kg]
Wheel Mass (M$_2$)	20 [kg]
Spring rate (k$_s$)	12000 [N/m]
Damping ratio (ξ)	0.25 [-]
Tyre stiffness (k$_t$)	143000 [N/m]

Seven-*DOF vehicle model parameters*

PARAMETER	VALUE
Sprung Mass (m)	1020 [kg]
Wheel Mass (m_1)	14.17 [kg]
Axle Mass (m_2)	30 [kg]
Pitch Moment of Inertia (J_α)	1859 [kgm^2]
Roll Moment of Inertia (J_β)	471 [kgm^2]
Axle Moment of Inertia ($J_{\beta"}$)	5.343 [kgm^2]
Front spring rate (k_1)	22000 [N/m]
Rear spring rate (k_2)	19000 [N/m]
Tyre stiffness (k_0)	143000 [N/m]
Viscous damper coefficient (c)	800 [Ns/m]
Tyre damping (c_0)	20 [Ns/m]
Centre of gravity (CG) distance from	1.025 [m]
CG distance from rear axle (b)	3.204 [m]
Axle length (E)	1.462 [m]
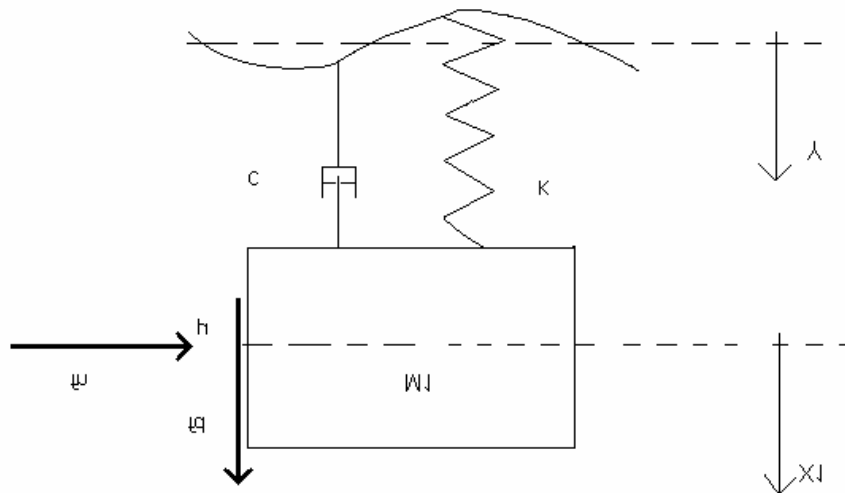
Figure 1
(NB: Figure captions at end of paper)
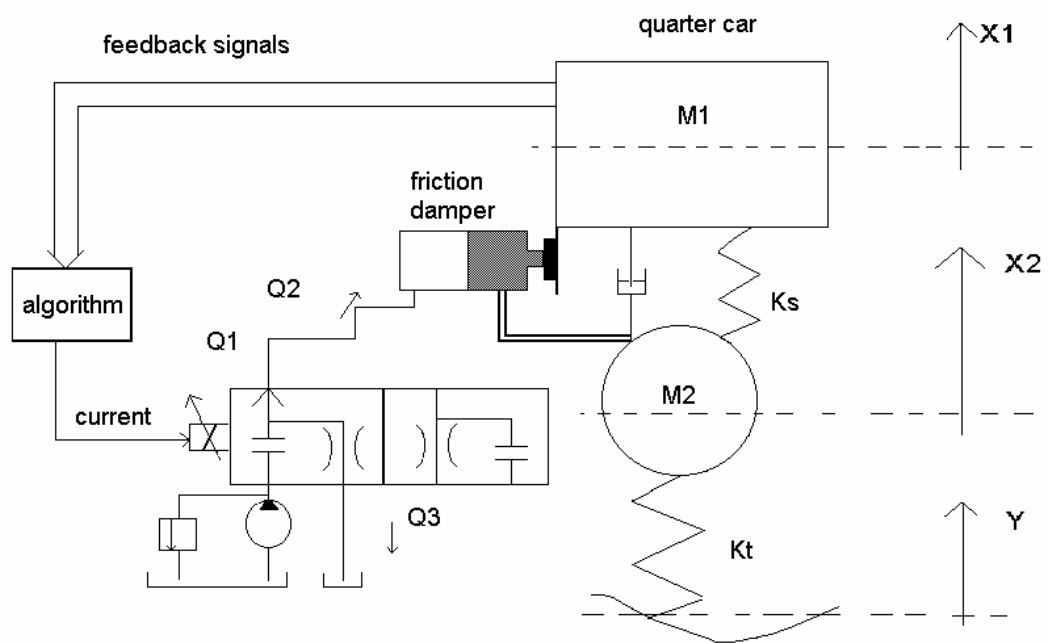
Figure 2
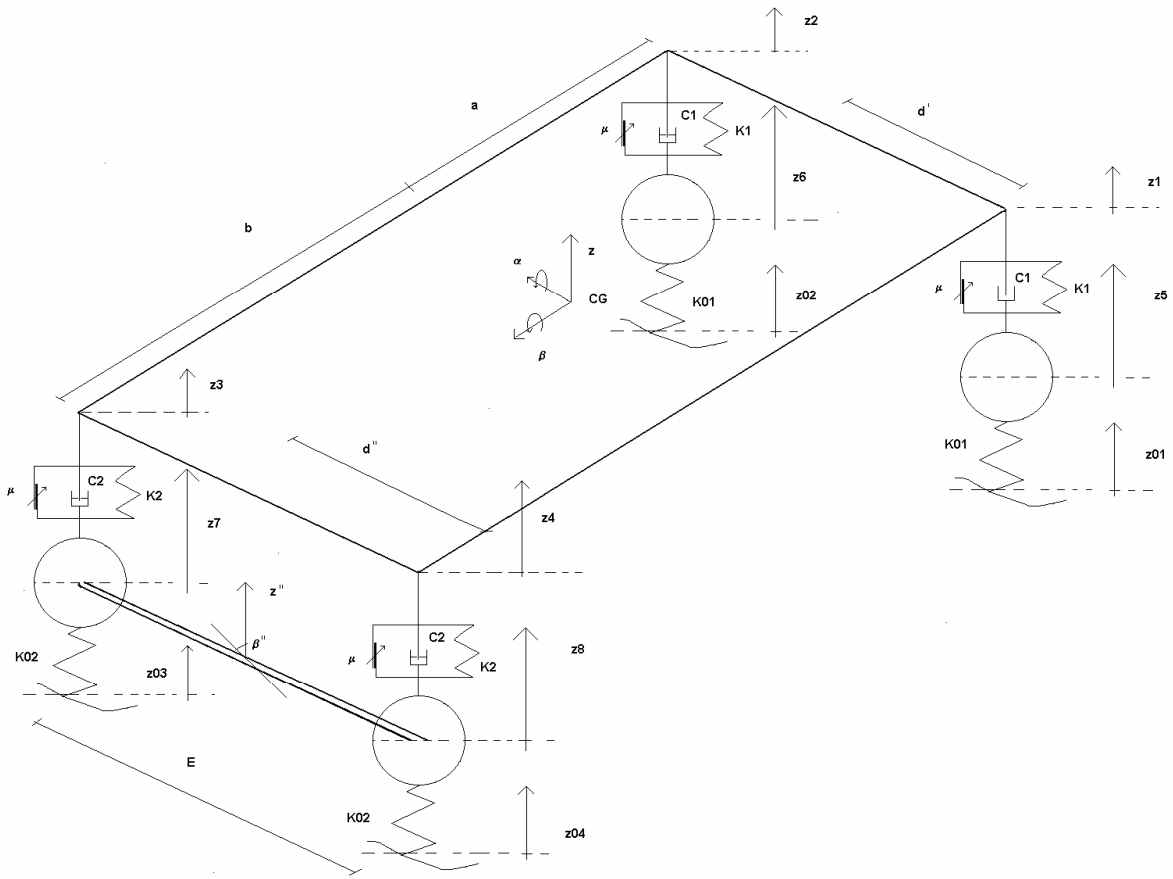
Figure 3

Figure 4

Figure 5

Hydraulic
Supply Port

Supply Pipe

Supply

Piston &
Friction
Pad

Detail of Friction
pad pistons
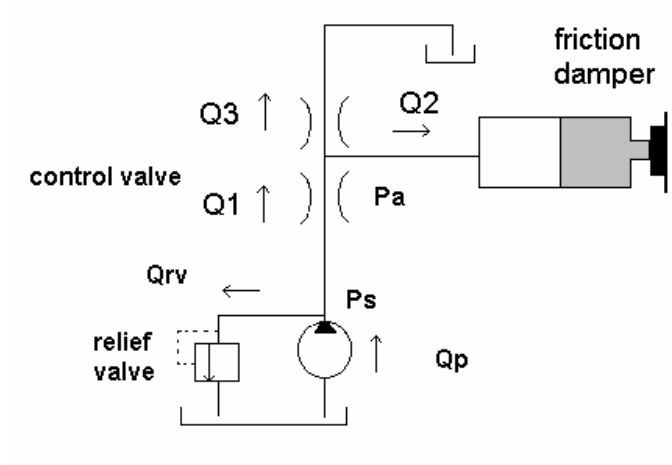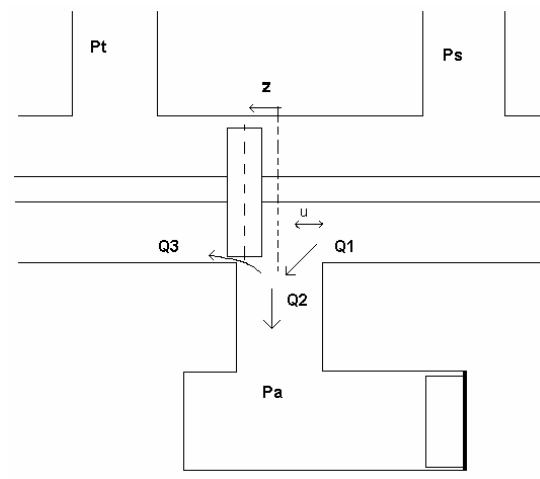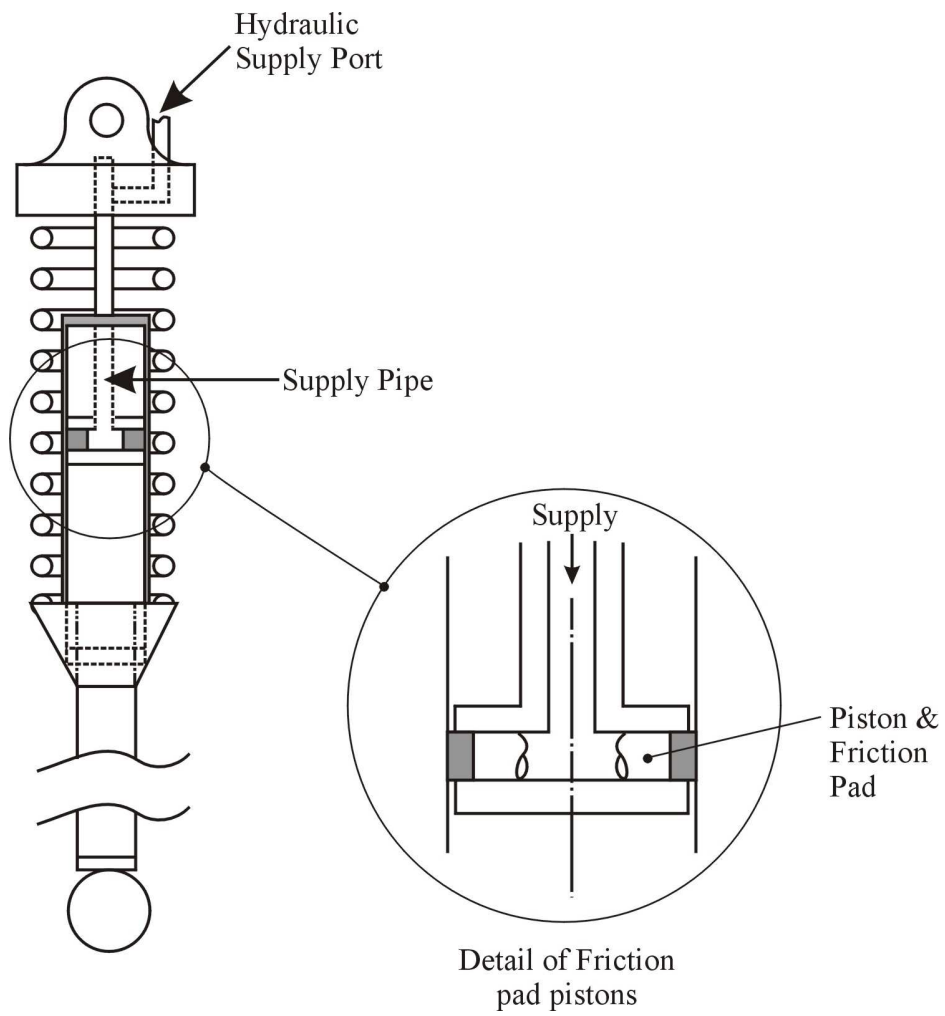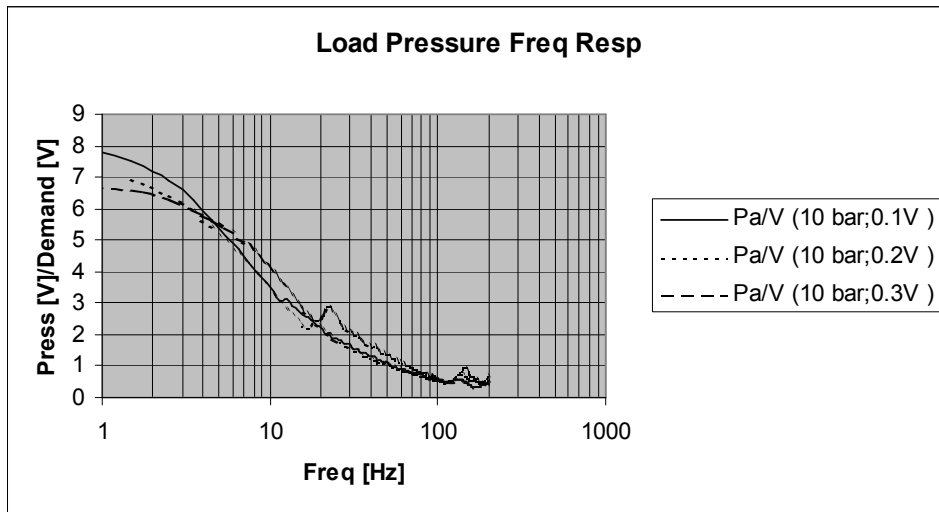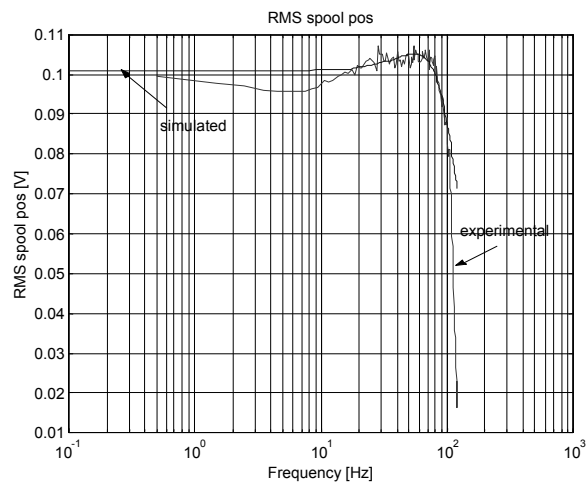
Figure 6

Figure 7

Figure 8
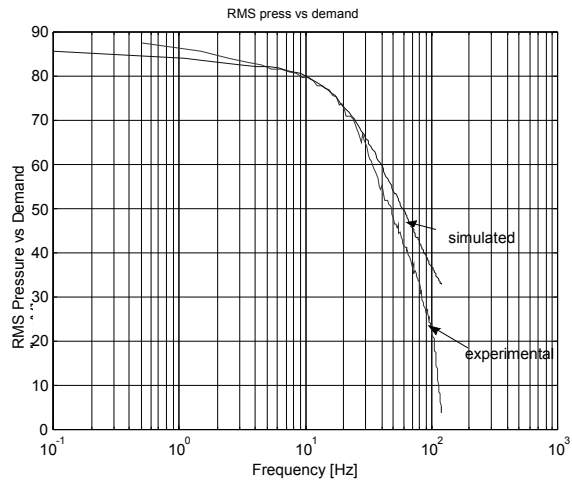
Figure 9
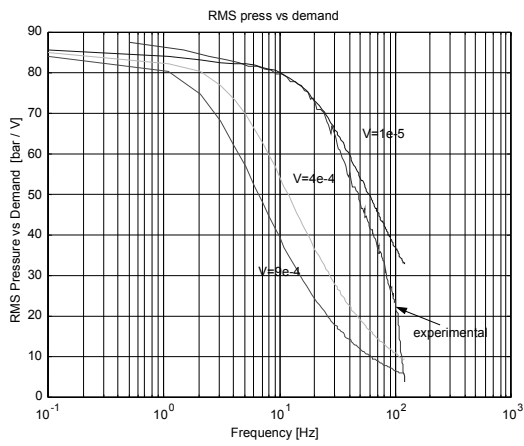
Figure 10
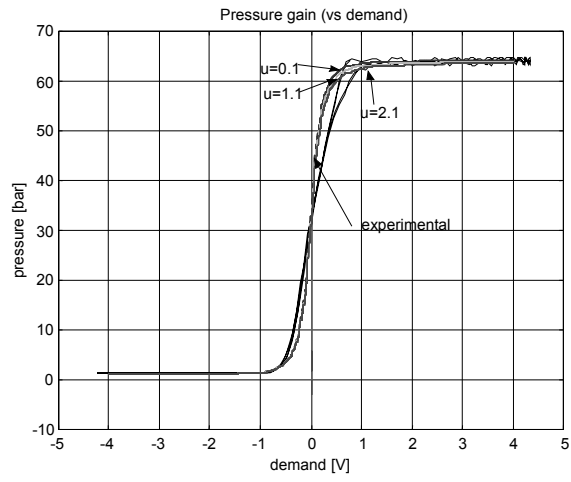
Figure 11
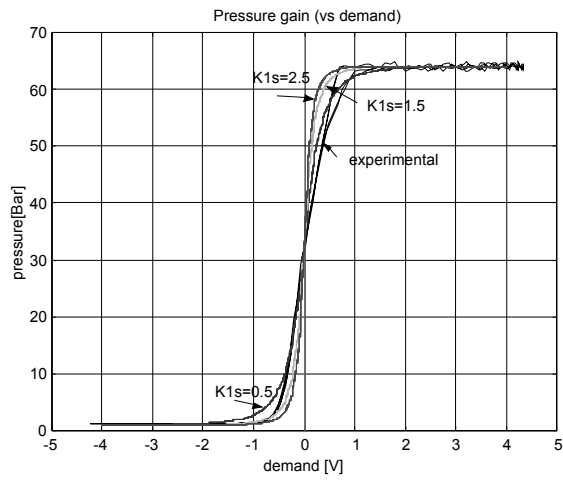
Figure 12
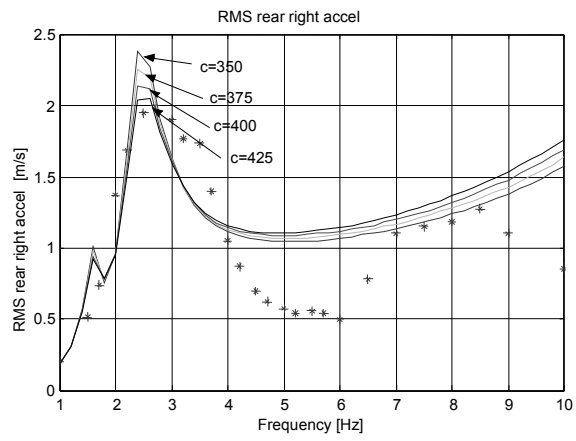
Figure 13
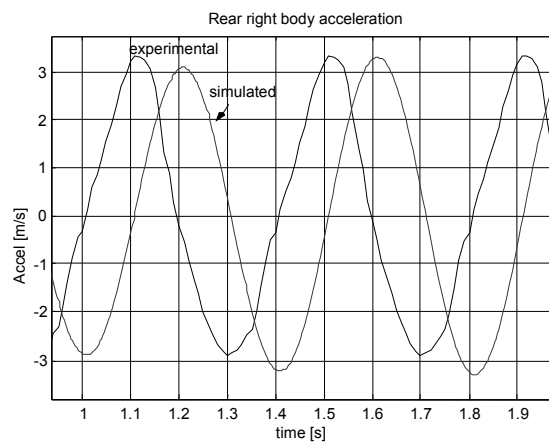
Figure 14
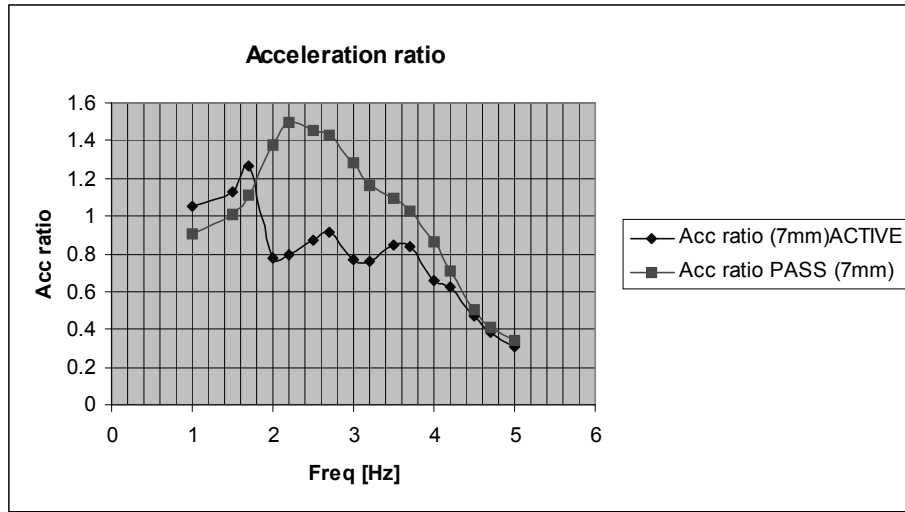
Figure 15
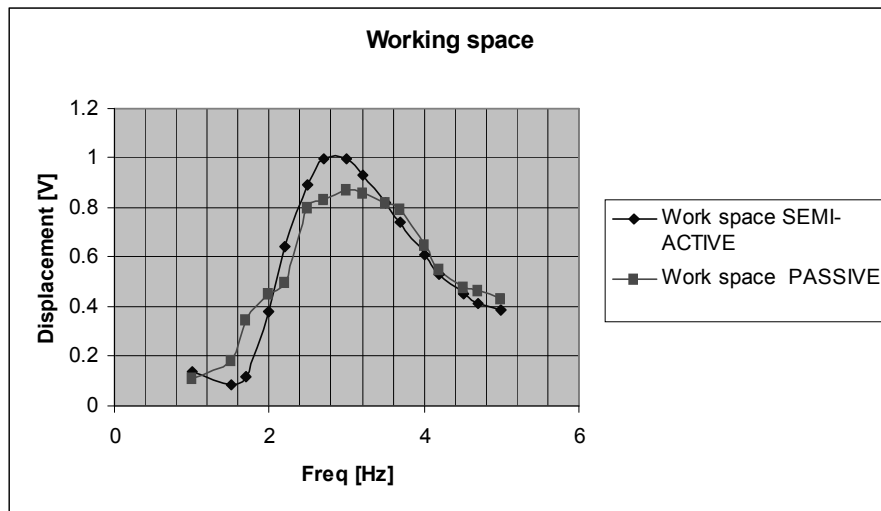
Figure 16
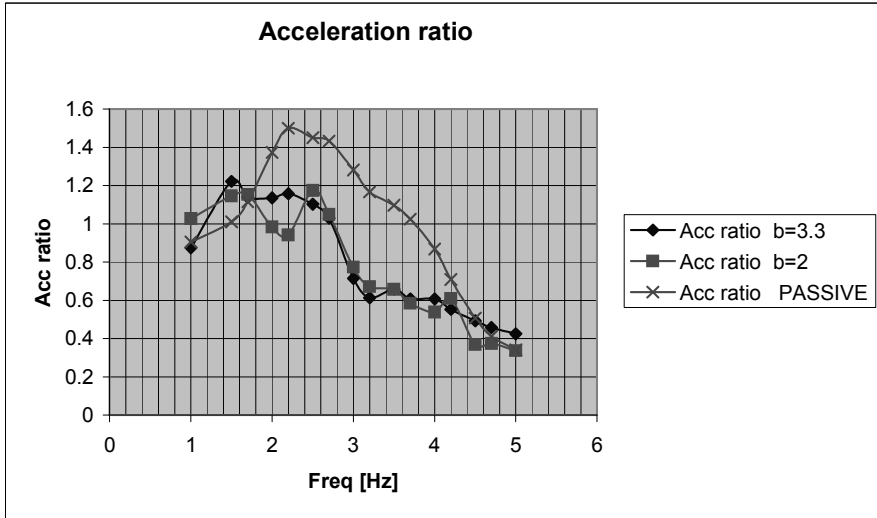
Figure 17
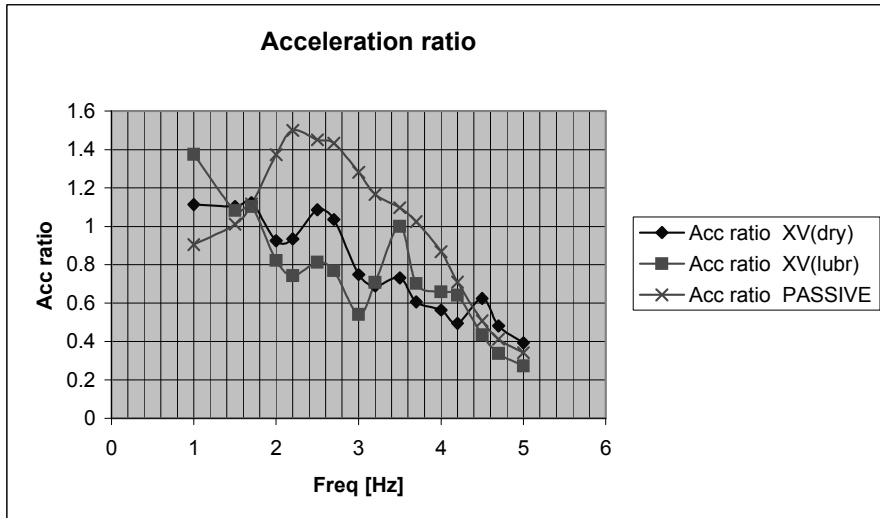
Figure 18
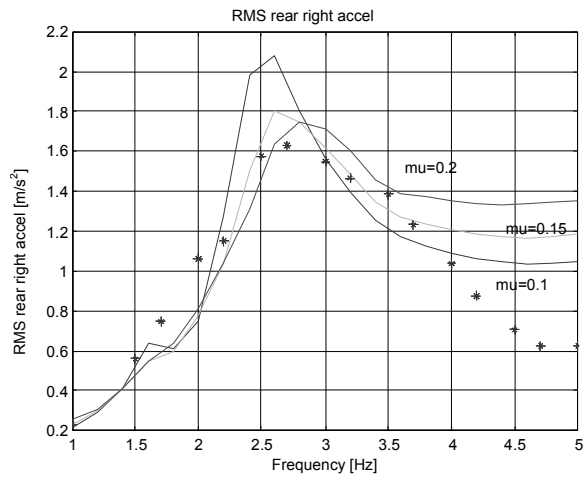
Figure 19
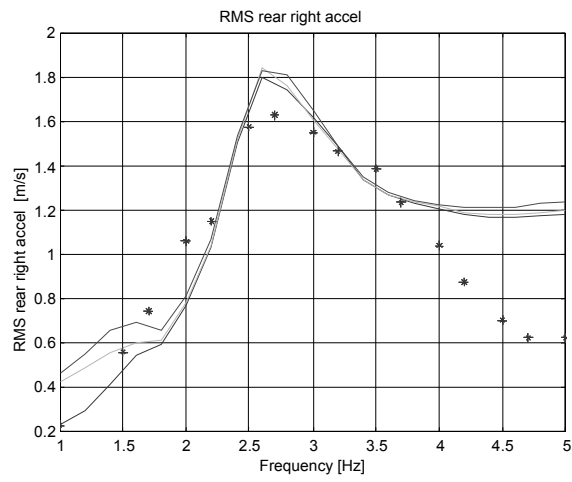
Figure 20
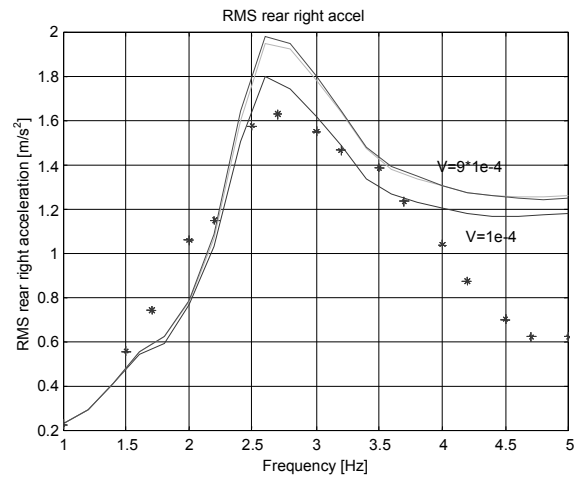
Figure 21
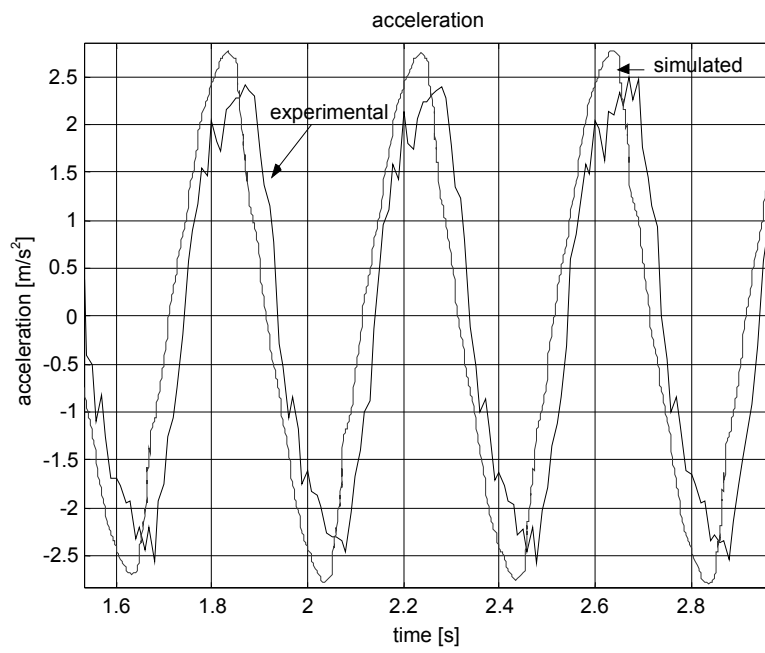
Figure 22

Figure 23

Figure 24

Figure 17 Acceleration transmissibility ratio for passive and semi-active systems; sinusoidal input to one wheel; amplitude: 7 mm

Figure 18 Acceleration transmissibility ratio with dry and lubricated friction; sinusoidal input to one wheel; amplitude: 7 mm

Figure 19 Rear right semi-active acceleration frequency response varying friction coefficient; sinusoidal input to one wheel; amplitude: 7 mm

Figure 20 Rear right semi-active acceleration frequency response with varying "frictional memory"; sinusoidal input to one wheel; amplitude: 7 mm

Figure 21 Rear right semi-active acceleration frequency response for different volumes (m^3); sinusoidal input to one wheel; amplitude: 7 mm

Figure 22 Rear right semi-active acceleration; sinusoidal input to one wheel; amplitude: frequency 2.5 Hz

Figure 23 Semi-active chassis acceleration time trend. Random input: 25 Hz filtered white noise

Figure 24 Bump response acceleration time trace for the semi-active system. Sinusoidal bump input; frequency 12 Hz, amplitude 30 mm.